JOURNAL OF OPTOELECTRONICS AND ADVANCED MATERIALS Vol. 12, No. 8, August 2010, p. 1720 - 1728

Tunable PbTe nanocolloids and nanolayers: HTSP precipitation, spectral properties and light-hole band lowering due to quantization

A. TODOSICIUC*, A. NICORICI, T. GUTSUL, F. GRAMM[a], L. BRAGINSKY[b], V. SHKLOVER[b]
Institute of Electronic Engineering and Nanotechnologies AS, Academiei str. 3/3, Chisinau 2028, Moldova
[a]*EMEZ – Electron Microscopy ETH Zürich, Wolfgang Pauli Strasse 16, 8093 Zurich, Switzerland,*
[b]*Laboratory of Crystallography, Department of Materials, ETH Zürich, Wolfgang Pauli Strasse 10, 8093 Zürich, Switzerland*

Colloidal suspensions of PbTe nanoparticles coated with oleic acid (OA) were obtained using a high-temperature solution phase (HTSP) method. Both diphenyl ether and squalane were used as high-boiling heat-transfer agents. It was shown that the change in standard synthesis conditions, such as the temperature of reaction and the group IV/group VI precursor molar ratio, led to precipitation of the nanocrystalline tellurium in parallel with PbTe nanoparticles. Bonding between the oleic acid and nanoparticles (NP) was investigated using Fourier transform infrared spectroscopy (FTIR) and X-ray photoelectron spectroscopy (XPS). The results indicated that oleic acid coordinated the nanoparticles symmetrically through carboxyl groups, and the interaction modes were bridging bidentate and chelating interactions. The strong coordination by the capping monolayer made the NP stable against oxidation. In contrast to bulk, nanocrystalline PbTe possesses photosensitivity to IR radiation at low temperatures enabling electrical conductivity, which itself has an activation character with rising temperature.

(Received June 11, 2010; accepted August 12, 2010)

Keywords: Lead telluride nanocrystals, HTSP synthesis, Colloidal solutions

1. Introduction

Lead-chalcogenide based solid solutions have attracted a great deal of interest over the last decade because of the possibilities for thermoelectric [1-4] and optoelectronic device [5-7] applications. The study of methods of synthesis for nanoscale lead chalcogenides is directed towards control of the dimensions and shape of nanoparticles during their nucleation and growth. Colloidal chemistry makes it possible to reduce the nanoparticle size to less than the excitonic Bohr radii, resulting in a size dependence on a number of nanoparticle properties [8]. Surfactant–assisted synthesis allows for adequate control of the size and shape of the particles during nucleation, growth and self-assembly, and is found to be successful in producing important semiconductor nanomaterials of the $A^{IV}B^{VI}$ class [9,10]. Nanocrystalline PbTe is a remarkable $A^{IV}B^{VI}$ semiconductor illustrated by the following reasons. It is a suitable and compliant material for nanoengineering due to the tunability of the size of nanocrystals, with the excitonic Bohr radius one order of magnitude larger. An extensive investigation of the various chemical routes has also revealed other strategies for shape tuning such as varying the precursor molar ratios, the type of surfactant, growth time, and other synthesis parameters. Control of the surface energy may result in cubic, octahedral, cuboctahedral and flower-shaped NP with a narrow size distribution. Interesting architectures, such as nanorods, nanowires, nanotubes and nanoboxes can also be obtained using electrochemical or solvothermal processes [11-14].

The present work focuses specifically on the influence of synthesis parameters, such as reaction temperature and TOP-Te/lead oleate molar ratio, on the final reaction products. Detailed FTIR measurements are used to investigate the coordination interaction between the stabilizing organic shell and nanoparticles. The optimum conditions of the high-temperature solution phase (HTSP) synthesis are selected to obtain nearly monodisperse PbTe nanoparticles, suitable for subsequent formation of conducting layers.

2. Experimental

Chemicals. Tri-*n*-octylphosphine (Aldrich, 90%), amorphous tellurium shot (Aldrich, 99.999%), squalane (Aldrich, 99%), diphenyl ether (DPE) (Fluka, 98%), lead acetate trihydrate (Aldrich, 99.99%), and oleic acid (cis-9-octadecenoic acid, Aldrich, 90%) were used as purchased without further purification. Anhydrous ethanol, hexane, chloroform, acetone, tetrachloroethylene, and trichloroethylene were purchased from different companies and used without further purification. Trioctylphosphine telluride (0.75 M, TOP-Te) was prepared by completely dissolving the necessary amount of tellurium in 50 ml of TOP at 60–70 °C with moderate

stirring. The TOP-Te solution described above was prepared and stored in a nitrogen glove box.

Synthesis. The HTSP method was used as the basis for preparing lead telluride nanoparticles. A detailed description of the PbTe synthesis has been previously published [15-18]. We performed two sets of HTSP syntheses with different high-boiling solvents. Diphenyl ether was selected as a solvent for the precursor mixture in the first series of the synthesis; the second synthetic set was carried out with squalane. A standard synthesis of PbTe semiconductor nanoparticles was performed in a round-bottom three-neck flask equipped with a magnetic stirrer, thermocouple, and temperature control unit. Lead oleate was prepared by heating a mixture of 0.758 g (2 mmol) lead acetate, 1.27 ml (4 mmol) of oleic acid, and 11.2 ml (20 mmol) of squalane or 20–25 ml of diphenyl ether. Oleic acid was employed both for group IV precursor formation and nanoparticle stabilization during the synthesis intended for nucleation and reaction rate control. This solution was heated under vacuum at 75–80 °C for 5–6 h in order to form lead oleate and remove already formed acetic acid. The subsequent synthesis of lead telluride nanoparticles was carried out by rapid injection of trioctylphosphine telluride (TOP-Te) solution, maintained at room-temperature, into a vigorously stirred mixture containing lead oleate heated from 140 °C to 200 °C under N_2 atmosphere.

Previous our investigations of the influence of precursor molar ratios on final synthesis products show that values of TOP-Te/lead oleate molar ratio within 1.5–2.5 yield high-quality PbTe nanoparticles and prevent precipitation of unreacted components. Synthesis routes based on TOP-Te/lead oleate molar ratio values ranged within 2.5–4.5 both with synthesis temperature and the time manipulations allowed the secondary precipitation of Te, together with PbTe nanoparticles. Thus, two parallel synthesis procedures, available through slightly adjusting the synthesis temperature and precursor molar ratios, can produce qualitative modifications of the end product. As was mentioned above, one of the synthesis procedures was based on diphenyl ether as a high-boiling organic solvent. The optimum amount of this solvent was determined for group VI precursor solutions, namely 3–3.5 mmol of Te solution per 10 ml of organic solvent. The reaction temperature was varied between 140 °C and 200 °C, and the TOP-Te/lead oleate molar ratio was selected as 2 : 1. The reaction mixture was then maintained at the fixed temperature for 10 min and then promptly cooled to room temperature using an ice-water bath. The solution quickly turned dark during the synthesis due to the formation of PbTe colloidal solution. The second synthesis set based on squalane as a high-boiling heat-transfer agent was carried out, and here the precursor molar ratios were different. The TOP-Te/lead oleate molar ratios varied from (2.5–4) to 1. After the injection of the TOP-Te solution, the reactions were maintained at 175 °C for 3 min to avoid the concomitant formation of the secondary products. The reaction mixture, which also turned dark quickly, was rapidly cooled to room temperature.

A solvent containing two parts of hexane, one part of anhydrous ethanol, and five parts of acetone was prepared to purify the nanoparticles from unreacted precursor, excess surfactant and high-boiling point solvents. A size-selective precipitation was carried out by centrifugation, using a polar/nonpolar solvent combination, consisting of acetone and either hexane or chloroform. After precipitation, the PbTe nanoparticles were isolated and re-suspended in chloroform, hexane, and trichloroethylene, followed by ultrasonic treatment to form stable colloidal solutions, used for further preparation and characterization. The chemical analysis and atomic absorption spectroscopy confirmed the PbTe composition of the nanomaterial deposited after multiple purifying and re-suspension of the original solution.

Nanocrystalline sample characterization. High-resolution transmission electron microscopy (HRTEM), powder X-ray diffraction (XRD), and infrared absorption spectroscopy (IR) were used to characterize the size, shape, structure, and composition of the PbTe nanocrystals and optical properties of the capping layer. The powder XRD data were recorded with CuKα radiation (λ=1.5406 Å) on a Scintag and PANanalytical X'Pert Pro diffractometers, both operating in the Bragg–Brentano geometry. Samples for the XRD measurements were prepared by the deposition of concentrated PbTe or PbTe/Te colloidal solutions in chloroform or trichloroethylene onto a glass substrate. The 2θ range scanned from 20° to 75°. A Philips CM 30 transmission electron microscope (TEM) equipped with a Super-Twin lens and LaB_6 emitter was used for HRTEM measurements. All the images were taken at 300 kV accelerating voltage and recorded with a megapixel CCD camera. The EDX spectra were collected on a Tecnai F30 TEM, operating at an accelerated voltage of 300 kV and equipped with a Schottky field emission electron source and a Super-Twin lens. Samples for the TEM were prepared by the deposition of a drop of dilute colloidal solution in chloroform, hexane, or trichloroethylene on a carbon-coated copper grid (200 mesh), allowing slow evaporation at room temperature. The IR absorption spectra were recorded with a VERTEX-70 Fourier transform spectrometer (Bruker Corp.). Each spectrum was obtained at room temperature by averaging over 64 interferograms with a resolution of 1 cm^{-1}. The samples for the IR measurements were prepared as pellets with KBr or CsI powders. The quantitative analysis of obtained nanopowders was performed on AAS-3 atomic absorption spectrometer using acetylene–air flame. The X-Ray photoelectron spectra were obtained using Physical Electronics Quantum 2000 instrument with a monochromatic Al$K\alpha$ source, capable of laterally resolving. The samples were prepared by pressing each nanopowder specimen into indium foil.

For the investigation of the obtained nanomaterial, products of the following synthesis parameters were selected: fixed reaction temperature T = 175°C, TOPTe/lead oleate molar ratio r = 2.5, 3.0, 3.5, and 4.0. Squalane was used as the high-boiling heat-transfer agent. For the second synthesis set, the following parameters

were specified: r = 2.0 for each synthesis, and T = 140, 160, 180, and 200 °C during the 10 min. Diphenyl ether was selected as a high-boiling solvent. As mentioned above, the samples prepared for X-ray powder diffraction by depositing the colloidal solution onto a glass substrate dropwise.

3. Results and discussion

The typical powder diffraction patterns of the PbTe nanolayers obtained at different temperatures in the presence of diphenyl ether are shown in Fig. 1. The nanomaterial exists in a single-phase and has a cubic close-packed structure. The peak positions correspond to polycrystalline PbTe. The average dimensions of the PbTe nanoparticles were estimated using the Scherrer equation[19] for the (200) peak: $L=K\cdot\lambda/\beta\cdot\cos\theta$. The estimated average size is 10 nm for nanoparticles obtained at 200 °C, 7.2 nm for nanoparticles obtained at 180°C, ~6.6 nm for nanoparticles obtained at 160°C, and less than 3 nm for nanoparticles synthesized at 140 °C. The correspondence between particle size estimated from XRD and that observed in TEM is quite good for the larger nanocrystals. The X-ray diffraction patterns of the nanomaterial synthesized with a higher molar ratio r in the presence of squalane, were also recorded.

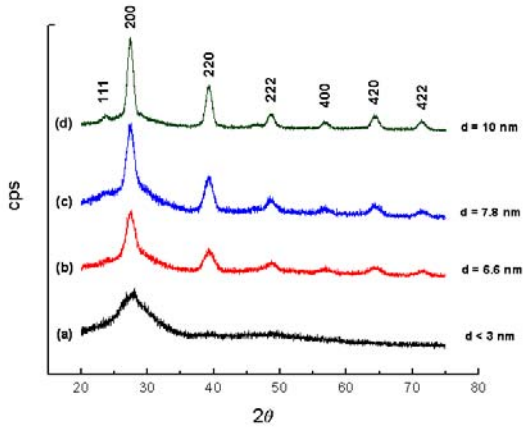

Fig.1. X-ray powder diffraction patterns of PbTe nanopowders synthesized in the presence of DPE at (a) T = 140 ºC; (b) T = 160 ºC; (c) T = 180 ºC; (b) T = 200 ºC.

All samples had a single-phase composition of lead telluride; the typical powder diffraction pattern of a PbTe nanolayer is shown in Fig. 2a. Fig. 2b shows the diffraction pattern of a nanolayer annealed at 500 °C. The appearance of the extraneous peaks (marked with asterisks (*)) in Fig. 2a is associated with residual precursors that are absent in X-ray patterns of annealed samples. An average size of 7.5 nm for the PbTe nanoparticles was estimated from the X-ray powder diffraction data using the Scherrer equation. After annealing at 500 °C, the average size of the nanoparticles increased to 35–40 nm, indicating sintering of the nanoparticles. Part of the reaction solution synthesized at the maximal group VI/group IV precursor molar ratio and maintained at room temperature for several hours, was also investigated, in addition to isolating and purifying nanoparticles from solution. Besides the presence of lead telluride, the precipitation of colloidal tellurium was detected and explained by irreversible chemical modifications in the initial contents of the reaction mixture occurring under the oxygen rich atmosphere.

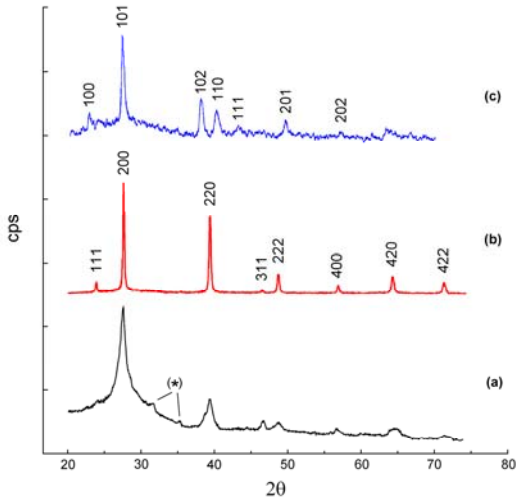

Fig. 2. X-ray powder diffraction patterns of (a) PbTe nanopowders obtained in the typical solution-phase synthesis and deposited on a glass substrate; (b) PbTe samples annealed at 500 ºC; (c) colloidal Te precipitated under modified synthesis conditions.

The precipitated product that remained indefinitely in the presence of oxygen was quantitatively analyzed by means of atomic absorption spectroscopy. It was observed that longer synthesis times with r values between 3.5–4.5 led to predominant Te formation (about 40–70% of the total amount of nanomaterial). The analysis of the X-ray diffraction data of the PbTe/Te nanolayers became complicated because of the uniform distribution of PbTe phase in the predominant Te phase. It was very difficult to observe the reflexes of the PbTe phase as the strongest (200) peak of PbTe coincides with the strong (101) peak of Te. Fig. 2c shows the diffraction pattern of the colloidal Te, precipitated in a synthesis with higher molar ratio r, after isolation of the primary reaction products. The average size of the Te nanoparticles was 20–25 nm. In a modified synthesis with higher reaction temperature, higher molar ratio r, and longer time for post synthesis procedures, a dramatic increase in the dimensions of Te nanoparticles were observed, accompanied by changes to a more rod-like shape (see Fig. 3d). This observation permitted us to combine the standard reaction conditions for PbTe synthesis with post synthesis procedures in order to simultaneously produce PbTe/Te nanomaterials. Nanoparticle size tuning was also attainable during both the synthesis of PbTe and Te nanoparticles and the post synthesis procedures. It is known that the shape of fcc

nanoparticles is determined basically by the growth rate in the <100> and <111> directions. Growth rates of the {100} and {111} facets with different surface energies vary during the nucleation and nanoparticle growth, and depend on the synthesis duration [16]. It should be noted that the presence of surfactants also influences the nanocrystal shape [20].

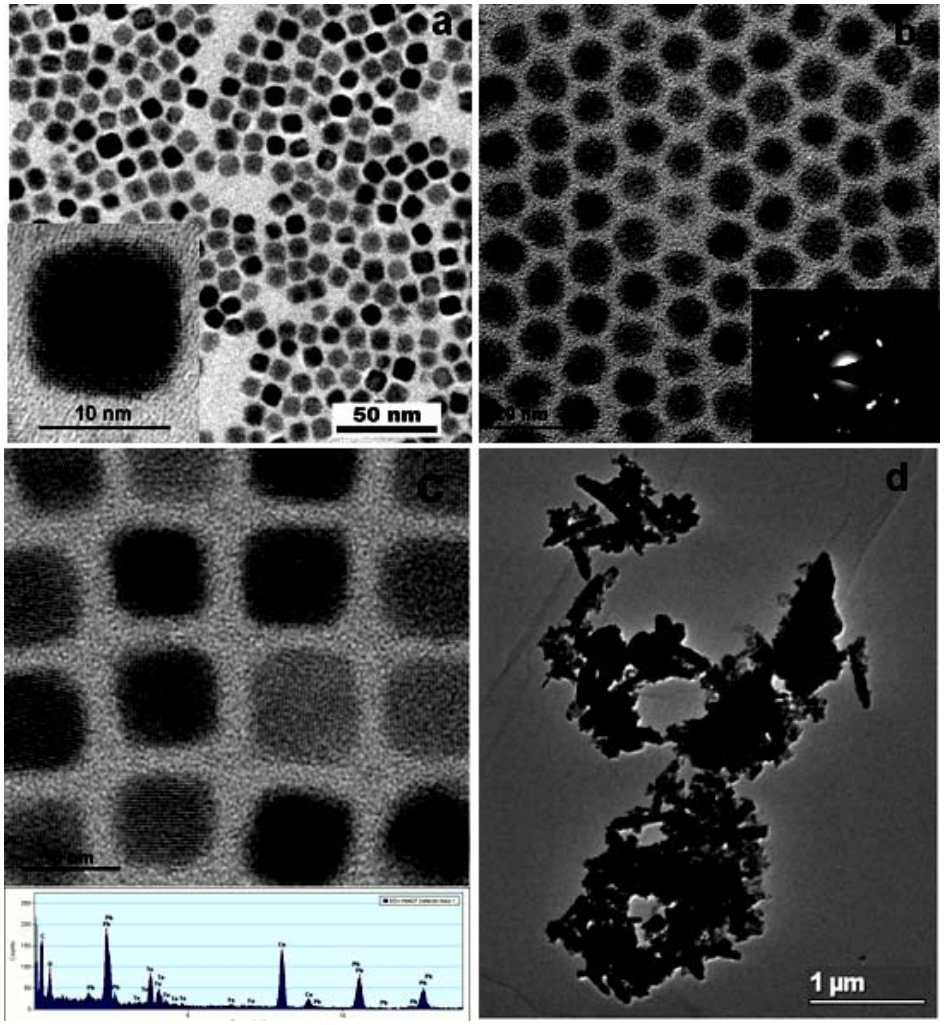

Fig. 3. Transmission electron micrographs of (a) PbTe nanoparticles obtained under typical synthesis based on DPE and reaction temperature 200℃, the inset shows representative HRTEM image of individual cubic nanocrystal; (b) spherical PbTe nanoparticles obtained at 180℃, the inset shows SAED pattern, demonstrating the crystallinity; (c) local ordered cubic nanocrystals (inset represents EDS spectrum); (d) Te nanorods surrounded by PbTe nanoparticles (precipitated at 180℃ during 20 min).

Size, shape, and crystallinity of NP were examined using TEM methods. Self-assembled PbTe nanopowders were brought from various solvents onto copper grids. TEM images represented in Figs. 3a-c show well-separated NP with an average size in agreement with the values calculated from the Scherrer equation. The EDX measurements (inset of Fig. 3c) confirmed the Pb:Te ratio of ~1. Fig. 3a shows the TEM image of the assembly of PbTe cubic nanoparticles with an average size of 10 nm, synthesized at 200 °C during 10 min in the presence of diphenyl ether. A HRTEM image shown in the inset of Fig. 3a confirms the high crystallinity of the single cubic nanoparticle. Local ordering of the cubic nanocrystals (Fig. 3c) into a close-packed structure indicates that the PbTe cubic nanoparticles have a well-defined shape and a narrow size distribution. As can be seen, the interparticle spacing of these close-packed structures is of ~2 nm. We can assume that each separated nanoparticle is surrounded by a surfactant monolayer. The PbTe nanoparticles synthesized at lower temperatures (150–180 °C) with the same precursor molar ratio and time of synthesis have a spherical shape and size of 7-8 nm diameter (Fig. 3b) and

could be assembled into a hexagonal long-range ordered array. The "spherical" nanoparticles have, in fact, cuboctahedral geometry with {100} and {111} growth facets. The faster growth rate of <111> facets eliminates them, and results in the formation of cubic-shaped nanoparticles. As was mentioned in Ref. [20] and [21], the growth rate in the <100> and <111> directions could be simultaneously tuned by balancing the choice of surfactant, precursor molar ratio, and time of synthesis, leading to cubic, cuboctahedral, or octahedral shapes. Under the synthesis conditions described above, the shape of the PbTe nanoparticles is determined by the reaction temperature. The TEM image of PbTe and Te nanoparticles obtained under high molar ratio *r* is presented in Fig. 3d. Te nanoparticles are rod-shaped and surrounded by PbTe nanoparticles. The size of Te rods is siginificantly larger than PbTe nanoparticles.

FTIR measurements were performed to study the PbTe nanoparticle–(oleic acid) interaction. Fig. 4 represents the IR absorption spectrum of pure oleic acid, and Fig. 5 shows absorption spectra of nanoparticles coated by oleic acid. The main peaks of IR spectrum of free oleic acid are attributed to the oleyl and carboxylic acid groups. Two intense peaks at 2925 cm^{-1} and 2854 cm^{-1} correspond to ν_{as} asymmetric and ν_s symmetric C–H stretching vibration of the CH_2 group, the band at 3005 cm^{-1} is assigned to the C–H stretching vibration in C=C–H *cis*-double bond. The absorption peaks related to the CH_2 deformation (scissoring) and bending (rocking) of multiple ($-(CH_2)_{n\geq 4}-$) methylene groups are specified at 1464 cm^{-1} and 724 cm^{-1}, respectively. The absorption peaks in the IR spectrum of pure oleic acid, having characteristics of a carboxylic acid group, are assigned as follows. The sharp band at 1711 cm^{-1} corresponds to C=O stretching mode; the band position at 1286 cm^{-1} indicates the presence of the C–O stretching vibrations of the carboxylic group. In addition, the carboxylic acid group possesses a broad O–H stretching band in the 3400–2500 cm^{-1} range, and the weak peak at 2674 cm^{-1} is specific for the O–H stretching mode of the oleic acid dimerized through the strong intermolecular hydrogen bonding [22-24]. The absorption peak observed at 935 cm^{-1} also corresponds to out-of-plane O–H bending vibrations of the dimerized oleic acid.

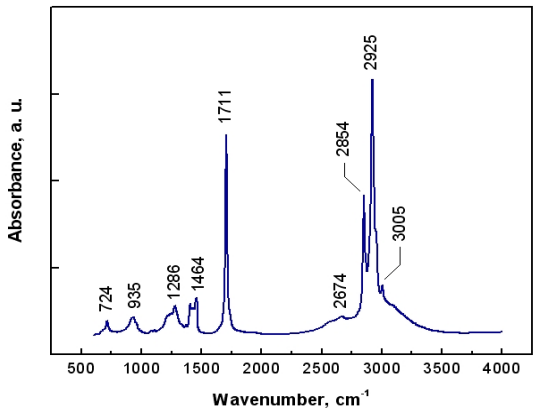

Fig. 4. FTIR spectrum of pure oleic acid.

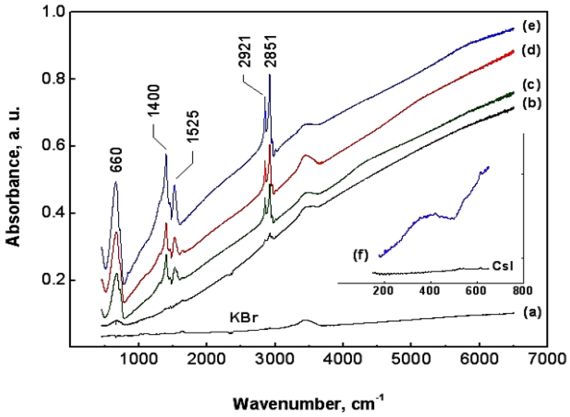

Fig. 5. FTIR absorption spectra of: (a) KBr pellet, (b) PbTe nanoparticles without the organic shell, (c),(d),(e) PbTe NPs synthesized at T = 200ºC, 180ºC, 160ºC, respectively. Inset (f) represents far IR spectrum of PbTe NPs.

Fig. 5 represents absorption spectra of the PbTe nanoparticles obtained at different synthesis conditions and passivated with oleic acid. These spectra exhibit considerable changes due to the interaction between the nanoparticle and capping layer. All spectra show a weak shift of the asymmetric and symmetric CH_2 stretch from its positions situated at 2925 cm^{-1} and 2854 cm^{-1} to lower wavenumbers of 2921 cm^{-1} and 2851 cm^{-1}, respectively[25]. The shoulder at 2955 cm^{-1} associated with the asymmetric stretching of the terminal CH_3 group of the alkyl chain becomes more pronounced as seen in Fig. 6a. The principal difference between the IR spectra of free oleic acid and coated nanoparticles is the disappearance of the sharp peak at 1710 cm^{-1} corresponding to the C=O stretching mode and growth of two new bands corresponding to the asymmetric $\nu_{as}(COO^-)$ stretch at 1525 – 1560 cm^{-1} and the symmetric $\nu_s(COO^-)$ stretch at 1400 cm^{-1} due to C=O bond rupture. These observations confirm the absence of the free oleic acid and permit us to assume that nanoparticle is surrounded by a relatively dense organic monolayer. Earlier investigations showed that the carboxylate groups interact with nanoparticle atoms, and the wavenumber difference between the asymmetric $\nu_{as}(COO^-)$ and symmetric $\nu_s(COO^-)$ bands could serve for estimating the mode of binding of carboxylate to the nanoparticle surfaces [26-29]. In our case, symmetric $\nu_s(COO^-)$ stretches are situated at 1400 cm^{-1}, and asymmetric $\nu_{as}(COO^-)$ stretches are situated both at 1525 and 1559 cm^{-1}. These two peaks that occur due to asymmetric COO^- stretches indicate that carboxylic group interacts with PbTe surface atoms via two different modes, and the prevalent interaction is characterized by a more intense peak at 1525 cm^{-1} of asymmetric COO^- stretches (Fig. 6b). Thereby, the wavenumber difference of $\Delta_1 \sim 125$

cm^{-1} corresponds to chelating via bidentate interaction, and Δ_2 ~ 159 cm^{-1} indicates the bridging bidentate interaction implicating that chelating interaction is predominant. These interactions mean that two oxygen atoms of the carboxylic group coordinate with one or two atoms of the nanoparticle (Scheme 1a, b). As seen from Figs. 5c-e, the strong peak around 660 cm^{-1} arises from the Te–O bond, and therefore tellurium atoms also participate in the coordination interaction with carboxylates. When Δ values discriminate between chelating ($\Delta \leq 110 - 115$ cm^{-1}) and bidentate ($\Delta > 140$ cm^{-1}) interactions, it is difficult to derive a concrete structural conclusion. This necessitates the consideration of a mixed coordination with bridging bidentate and chelating interaction.

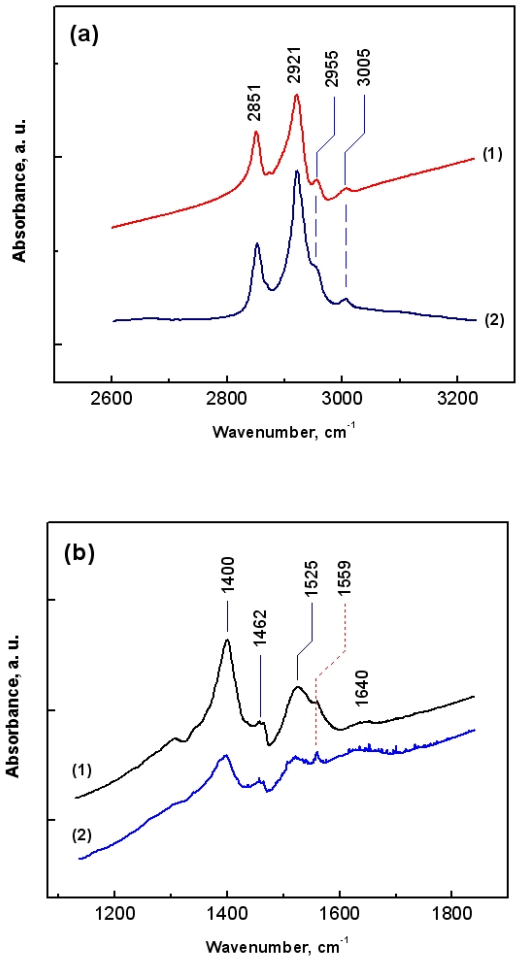

Fig.6. Absorption bands showing presence of: (a) CH_2 and CH_3 groups, curve (1) represents FTIR absorption spectra of PbTe NPs coated with OA, curve (2) represents the same spectra of free OA; (b) COO^- group, curves (1) and (2) represent FTIR spectra of PbTe NPs with moderate and intensive capping.

The FTIR spectra of the PbTe nanoparticles stabilized with an organic coating are quite similar and almost do not depend on synthesis conditions. After the removal of the coordinating organic shell, a dramatic decrease of intensity of the absorption bands occurred (Fig. 5b). However, the IR absorption spectra of the nanocrystals remained unchanged. Far IR absorption spectra of coated nanoparticles are shown in Fig. 5f. We assigned the band at around 400 cm^{-1} to a weak coordination bonding of the carboxylates to lead atoms.

X-ray photoelectron spectroscopy was also used to examine the chemical composition of surfactant-assisted PbTe nanocrystals. All the samples tracked exhibit the same spectra, and the typical binding energies of O 1s, C 1s, Pb 4f, and Te 3d core levels are presented in Fig. 6. The single O1s characteristic peak at 530.2 eV might be interpreted as carboxylate (COO^- moiety) oxygen atoms that have symmetric spacing and exclude the C=O bond in the organic coverage of PbTe nanoparticles. This also confirms the absence of free oleic acid and excludes monodentate coordination of carboxylate to the nanoparticle surface. Fig. 6b represents the C 1s photoelectron spectrum comprised of two C1s peaks occurred at 284.9 and 288.3 eV, which correspond to the carbon atoms in the aliphatic chain and the carboxylate moiety, respectively. The photoelectron spectrum of Pb 4f has a doublet with binding energies of 138.0 and 142.9 eV, assigned to Pb $4f_{7/2}$ and Pb $4f_{5/2}$ sub-bands, shown in Fig. 7c. The shoulder peaks of the Pb 4f doublet corresponding to a chemical shift to a higher binding energy as a result of NP surface oxidation were not found.

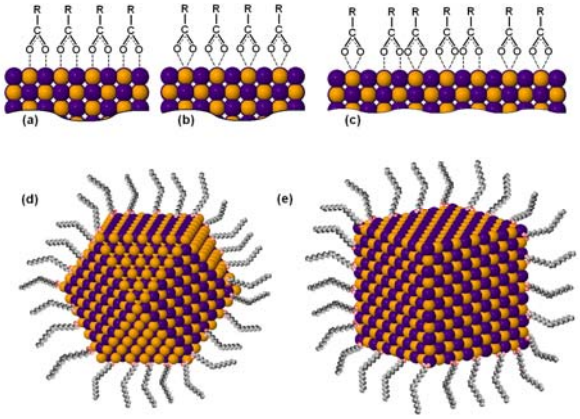

Scheme 1. Simplified models of: (a) bridging bidentate interaction between the carboxylic group and PbTe nanoparticle, (b) chelating interaction, (c) both bridging bidentate and chelating interaction between the capping layer and nanoparticle, (d, e) schematic representation of the single cubic and cuboctahedral nanoparticle passivated with oleic acid.

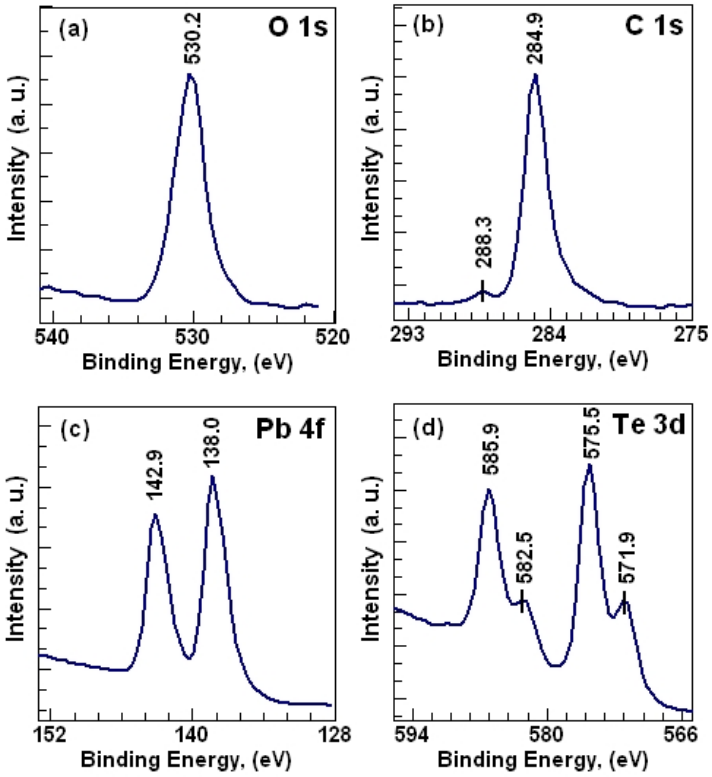

Fig.7. XPS spectra of the surfactant-coated PbTe nanoparticles.

The first striking result from the Te 3d XPS spectrum is that the two doublets reveal two chemically different states of Te (Fig. 6d). The Te 3d doublet with binding energies of 582.5 eV and 571.9 eV, corresponding to Te $3d_{3/2}$ and Te $3d_{5/2}$ sub-bands, imply the binding of the Te atoms situated in the nanoparticle core, while the more intense doublet with the binding energies of 585.9 and 575.5 eV appears due to Te surface atom participation in the Te–O bonding with carboxylates. Reconstruction of the tellurium and oxygen electronic clouds (C=O bond opening) results in coordination bond formation whose strength approaches covalent bonding. The fact that a moiety of cuboctahedral shaped nanoparticles has Te-terminated {111} facets (Te reached NP surface) both with chelating and bidentate interaction with chemisorbed oleic acid permits us to assume that the change in the Te surface chemical states has both a size and shape aspect.

Initially, the PbTe nanolayers deposited from diluted solutions had low electrical conductivity due to the organic covering, but the conductivity can be greatly enhanced at room temperature by dissolving this organic shell with chloroform. Some authors have applied special methods to increase electrical conductivity, such as chemical activation, annealing, etc [9, 10]. The temperature dependence of the electrical conductivity of PbTe nanolayers is shown in Fig. 8. As one can see, it has the activation energy of ΔE_a = 0.23 eV, but at low temperatures (T < 200 K) it is only ΔE_a = 0.011 eV. In addition to the enhanced electrical conductivity, PbTe nanolayers are photosensitive to IR radiation at 77 K, the photosensitivity being of the same order of magnitude as that of PbTe-based solid solutions at lower temperatures of 20–30 K.

The most interesting aspect of the absorption (Fig. 5) is its linear dependence on the wavenumber and, therefore, on the photonic frequency ω. To understand this, note that the observed nanoparticle size of d = 6.5 nm means that each particle contains over 2000 atoms, every second of them is situated at the nanoparticle surface. This means that the model of direct interband absorption no longer holds, and the indirect electron transitions must be taken into account. This leads to the following dependence on the light frequency[31]

$$\eta \propto (\hbar\omega - E_g)^{\nu},$$

where ν = 1 in the presence of the structure resonance in both bands between which the interband absorption occurs, i.e., if these bands are close to the extended or interface states of the matrix material. The availability of the interface states in the conduction band is illustrated in Fig. 5 by two peaks at 1400 cm^{-1} and 1525 cm^{-1}. The valence bands of PbTe and the matrix material must be close, because they are responsible for the chemical bonding. Let us estimate the shift of the valence and

conduction bands due to the size quantization. The effect is

$$\Delta E = \frac{\pi^2\hbar^2}{2md^2}.$$

Effective masses of electrons and holes in PbTe are quite anisotropic. Assuming $m = 0.02m_e$ (smallest value of the effective mass) and the particle size of d = 6.5 nm, we obtain ΔE = 0.33 eV. This is close to the difference between the tops of L and Σ hole bands (0.3 eV). This means that the light-hole band lowers

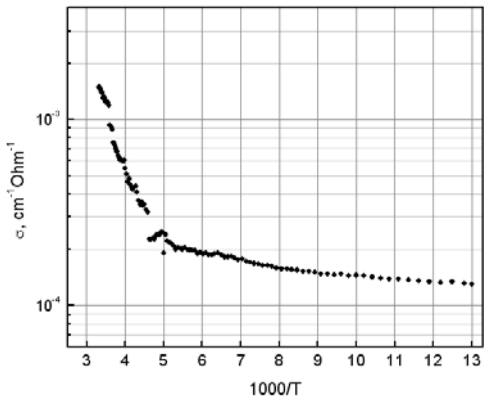

Fig. 8. Measured temperature dependence of the electrical conductivity of PbTe nanolayers.

due to the size quantization, and the excitation occurs mainly from the heavy-hole band. This should appreciably increase the absorption due to large effective mass and, therefore, lead to higher density of states in this band.

4. Conclusions

The influence of the modified synthesis conditions, such as an increase in the TOP-Te/lead oleate molar ratio, on PbTe synthesis was studied. The precipitated product was analyzed quantitatively by atomic absorption spectroscopy; it was shown that in addition to PbTe formation, co-precipitation of Te nanoparticles and PbTe nanoparticles occurred. Size tuning and shape evolution were realized by the change of reaction temperature. As-synthesized PbTe and PbTe/Te nanoparticles were stabilized with a dense monolayer of the oleic acid and formed stable colloidal suspensions. The stabilization of nanoparticles took place via coordination by the COO^- carboxylic groups of oleic acid. The FTIR measurements indicate that the coordination is of bidentate chelating type, each oxygen atom of the carboxylic group symmetrically coordinates the nanoparticle. Thus, the capping layer form part of the common structure with nanoparticles and makes it possible to control the nucleation growth of nanoparticle during the synthesis. XPS and FTIR measurements also demonstrate that the modifications of the surface states occurred; neither free surfactant nor high-boiling solvents were present in precipitated and purified nanoparticles. The nanopowders were photosensitive to IR radiation at low temperatures had the temperature dependent electrical conductivity with an activation energy of ΔE_a = 0.23 eV. Theoretical estimation shows that the light-hole band lowered due to the size quantization, and the excitation occurred mainly from the heavy-hole band.

Acknowledgments

The work was supported by the SCOPES program of the Swiss National Science Foundation, project No. IB7320-110921 / 1. The authors are indebted to Dr. J. Patscheider (Swiss Federal Institute of Material Testing) for recording XPS spectra.

References

[1] L. D. Hicks, M. S. Dresselhaus, Phys. Rev. B **47**, 12727 (1993)
[2] T. C. Harman, P. J. Taylor, M. P. Walsh, LaForge, B. E. Science **297**, 2229 (2002)
[3] J. P. Heremans, C. M. Thrush, D. T. Morelli, Phys. Rev. B **70**, 115334 (2004)
[4] V. V. Shchennikov, S. V. Ovsyannikov, Solid State Commun. **126**, 373 (2003)
[5] B. A. Volkov, L. I. Ryabova, D. R. Khokhlov, Physics – Uspekhi, **45**(8), 819 (2002)
[6] S. N. Chesnokov, D. E. Dolzhenko, I. I. Ivanchik, D. R. Khokhlov, Infrared Phys. **35**, 23 (1994)
[7] D. R. Khokhlov, I. I. Ivanchik, S. N. Raines, D. M. Watson, J. L. Pipher, Appl. Phys. Lett. **76**, 2835 (2000)
[8] L. E. Brus, J. Chem. Phys. **80**, 4403 (1984)
[9] J. J. Urban, D. V. Talapin, E. V. Shevchenko, C. B. Murray, J. Am. Chem. Soc. **128**, 3248 (2006)
[10] M. V. Kovalenko, W. Heiss, E. V. Shevchenko, J.-S. Lee, H. Schwinghammer, A. P. Alivisatos, D. V. Talapin, J. Am. Chem. Soc. **129**, 11354 (2007)
[11] G. Zhang, X. Lu, W. Wang, X. Li, Chem. Mater., **19**, 5207 (2007)
[12] W. Wang, B. Poudel, D. Wang, Z. F. Ren, Adv. Mater. **17**, 2110 (2005)
[13] Y. Yang, S. C. Kung, D. K. Taggart, C. Xiang, F. Yang, M. A. Brown, A. G. Guell, T. J. Kruse, J. C. Hemminger, R. M. Penner, Nano Lett. **8**, 2447 (2008)
[14] J. Zhang, A. Kumbhar, J. He, N. C. Das, K. Yang, J.-Q. Wang, H. Wang, K. L. Stokes, J. Fang, J. Am. Chem. Soc. **130**, 15203 (2008)
[15] J. E. Murphy, M. C. Beard, A. G. Norman, P. S. Ahrenkiel, J. C. Johnson, P. R. Yu, O. I. Micic, R. J. Ellingson, A. J. Nozik, J. Am. Chem. Soc. **128**, 3241 (2006)
[16] W. G. Lu, J. Y. Fang, K. L. Stokes, J. J. Lin, Am. Chem. Soc. **126**, 11798 (2004)
[17] G. F. Zou, Z. P. Liu, D. B. Wang, C. L. Jiang, Y. T. Qian, Eur. J. Inorg. Chem. 4521 (2004)
[18] C. B. Murray, D. J. Norris, M. G. Bawendi, J. Am. Chem. Soc. **115**, 8706 (1993).
[19] H. P. Klug, L. E. Alexander, X-Ray Diffraction Procedures for Polycrystalline and Amorphous

Materials John Wiley & Sons: New York, p. 491 (1962).
[20] T. Mokari, M. Zhang, P. Yang, J. Am. Chem. Soc. **129**, 9864 (2007)
[21] Y. Sun, Y. Xia, Science **298**, 2176 (2002)
[22] B. Smith, Infrared Spectral Interpretation: A Systematic Approach, CRC Press: Boca Raton, p. 98 (1999)
[23] T. V. Vijaya Kumar, S. Prabhakar, G. J. Bhaskar Raju, Colloid Interface Sci. **247**, 275 (2002)
[24] N. Shukla, C. Liu, P. M. Jones, D. Weller, Journal of Magnetism and Magnetic Materials **266**, 178 (2003)
[25] L. H. Dubois, B. R. Zegarski, R. G. Nuzzo, Langmuir **2**, 412 (1986)
[26] M. Wuhn, J. Weckesser, C. Woll, Langmuir, **17**, 7605 (2001)
[27] G. B. Deacon, R. J. Philips, Coord. Chem. Soc. 1912. (1973)
[28] Y. Ren, K. Limura, T. Kato, Langmuir **17**, 2688 (2001).
[29] K. Nakamoto, Infrared and Raman spectra of inorganic andcoordination compounds; John Wiley & Sons: New York, p. 59 (1997)
[30] J. Pola, M. Urbanova, E. A. Volnina, S. Bakardjieva, J. Subrt, Z. Bastl, J. Mater. Chem. **13**, 394 (2003)
[31] L. S. Braginsky, Physical Review B **57**, 12. (1998)

*Corresponding author:alexandr.todosiciuc@mat.ethz.ch